The Pathogenesis of Retinal Damage in Blunt Eye Trauma: Finite Element Modeling

Tommaso Rossi,[1] *Barbara Boccassini,*[2] *Luca Esposito,*[3] *Mario Iossa,*[1] *Andrew Ruggiero,*[3] *Ciro Tamburrelli,*[1] *and Nicola Bonora*[3]

Purpose. To test the hypothesis that blunt trauma shockwave propagation may cause macular and peripheral retinal lesions, regardless of the presence of vitreous. The study was prompted by the observation of macular hole after an inadvertent BB shot in a previously vitrectomized eye.

Methods. The computational model was generated from generic eye geometry. Numeric simulations were performed with explicit finite element code. Simple constitutive modeling for soft tissues was used, and model parameters were calibrated on available experimental data by means of a reverse-engineering approach. Pressure, strain, and strain rates were calculated in vitreous- and aqueous-filled eyes. The paired *t*-test was used for statistical analysis with a 0.05 significance level.

Results. Pressure at the retinal surface ranged between −1 and +1.8 MPa at the macula. Vitreous-filled eyes showed significantly lower pressures at the macula during the compression phase ($P < 0.0001$) and at the vitreous base during the rebound phase ($P = 0.04$). Multiaxial strain reached 20% and 25% at the macula and vitreous base, whereas the strain rate reached 40,000 and 50,000 seconds^{-1}, respectively. Both strain and strain rates at the macula, vitreous base, and equator reached lower values in the vitreous- compared with the aqueous-filled eyes ($P < 0.001$). Calculated pressures, strain, and strain rate levels were several orders of magnitude higher than the retina tensile strength and load-carrying capability reported in the literature.

Conclusions. Vitreous traction may not be responsible for blunt trauma–associated retinal lesions and can actually damp shockwaves significantly. Negative pressures associated with multiaxial strain and high strain rates can tear and detach the retina. Differential retinal elasticity may explain the higher tendency toward tearing the macula and vitreous base. (*Invest Ophthalmol Vis Sci.* 2011;52:3994–4002) DOI:10.1167/iovs.10-6477

Blunt eye traumas comprise all closed-globe injuries in which mechanical deformation and/or direct energy delivery causes tissue damage.[1] They account for more than 60%[2] of the estimated 2.4 million eye injuries per year in the United States alone.[3] Retinal sequelae of blunt trauma span a variety of well-known conditions, including commotio retinas (Berlin's edema),[4] choroidal rupture,[5] retinal tears, retinal detachment, dialyses,[6] and macular hole (MH).[7]

While clinical presentation of retinal and choroidal lesions has been thoroughly described, the pathogenic mechanism is still incompletely understood.[8] The most accepted theory postulates that vitreous traction is the main cause of retinal damage,[9] whereas alternative explanations suggest other mechanisms, such as differential globe layer deformation and increased internal limiting membrane (ILM) stiffness.[10]

Finite element modeling (FEM) is a numerical analysis approach, routinely used to simulate multiphysics problems involving complex structures and loading conditions. FEM has been applied to biological systems, specifically to the eye, to simulate the stress–strain response of the lamina cribrosa,[11] the cornea,[12] and the whole eyeball.[13]

The purpose of the present paper was to report an FEM analysis of a standardized blunt eye trauma and verify the hypothesis that shockwave-generated pressure and strain may be responsible for the retinal damage, regardless of the presence of the vitreous.

The study was prompted by the anecdotal observation of a traumatic MH in a previously vitrectomized eye, where no vitreous traction process could be invoked as the governing damage mechanism.

Materials and Methods

Case Report

A 54-year-old white male was referred to our emergency room complaining of abrupt loss of vision after being inadvertently shot in his right eye with a BB[14] gun. The right eye had had successful surgery 3 years earlier for primary pars plana vitrectomy and gas exchange by one of us (TR), due to rhegmatogenous retinal detachment, and had a best corrected visual acuity of 20/25 at his latest follow-up visit, 4 months earlier.

On presentation, right eye visual acuity (OD VA) was count fingers, slit lamp examination showed a corneal abrasion, 2 mm hyphema, 2+ Tyndall in the anterior chamber, and an intraocular lens well positioned within the capsular bag. A fundus view showed an attached retina, a slightly hyperemic optic nerve, and a small MH (Fig. 1), with surrounding retinal edema of the posterior pole. The temporal preequatorial retina also appeared mildly edematous.

One month later, OD VA had improved to 20/40, and a full-thickness MH was still visible although decreased in size. MH surgery was withheld, and 6 months later, VA was 20/30 with spontaneous MH closure.

FEM Model

The generic human eye was derived from anatomic observation[15] (Fig. 2A) and surface geometry, and thickness data were combined to generate an FE mesh modeler (Truegrid; XYZ Scientific Application, Inc., Livermore, CA). A finite element model using eight-node brick elements was been built for the cornea, sclera, crystalline

From the [1]Ospedale Ospedale Oftalmico di Roma, Rome, Italy; [2]Fondazione G. B. Bietti, IRCCS (Istituto Ricerca e Cura a Carattere Scientifico), Rome, Italy; and the [3]Department of Mechanics, Structure, and Environment (DiMSAT), University of Cassino, Cassino, Italy.

Submitted for publication August 26, 2010; revised January 8, 2011; accepted January 25, 2011.

Disclosure: **T. Rossi**, None; **B. Boccassini**, None; **L. Esposito**, None; **M. Iossa**, None; **A. Ruggiero**, None; **C. Tamburrelli**, None; **N. Bonora**, None

Corresponding author: Tommaso Rossi, Via Tina Modotti 93, 00142 Rome, Italy; tommaso.rossi@usa.net.

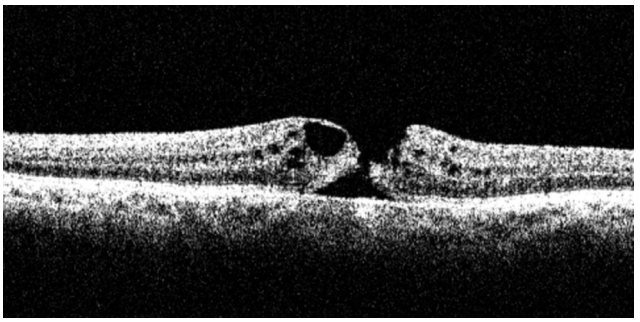

FIGURE 1. OCT image of a traumatic macular hole. Note the hyporeflective intraretinal cysts due to retinal edema, the presence of a very limited perilesional detachment, and the interruption of the ILM and the inner–outer segment (IS/OS) line. No vitreous–retina interface is visible in this vitrectomized eye.

lens, vitreous, and retina (Figs. 2B, 2C). All parts of the eye have been assumed to be connected. Half of the globe has been modeled assuming symmetry around the visual axis. The BB was modeled as a rigid solid half sphere with 4.5-mm diameter and 0.345/2 g weight, impacting the cornea at a speed of 62.5 m/s perpendicular to the corneal apex, according to the experimental conditions described by Delori et al.[9]

The decision to replicate the experiment of Delori et al. resides in the outstanding quality of the setting and the exquisite detail of their published data, which created a true gold standard in ocular traumatology.

Constitutive Models and Mechanical Properties

Numerical simulations were performed with commercial software (MSC.DYTRAN 2008r1; MSC Software, Santa Ana, CA). The code is an explicit finite element analysis solution developed for complex nonlinear behavior involving permanent deformation of structures. Simulations were performed with a Lagrangian solver (finite element). A preliminary model sensitivity analysis was performed, and adequate numerical accuracy was achieved with 6912 brick elements (technical specifications reported in Table 1).

The sclera, cornea, and retina were modeled as linear elastic materials, whereas the crystalline lens and vitreous were modeled with a linear equation of state, for hydrostatic pressure dependence, and the generalized Maxwell viscoelastic model, for the deviatoric response.

$$\sigma'_{ij}(t) = 2\int_0^t G_0 \exp[-\beta(t-\tau)]\frac{\partial \varepsilon'_{ij}(\tau)}{\partial \tau}d\tau + G_\infty \varepsilon'_{ij}(t) + 2\eta_0\frac{\partial \varepsilon'_{ij}(t)}{\partial t}$$

where σ'_{ij} and ε'_{ij} are the deviatoric stress and strain tensors, G_∞ is the saturated shear module, G_∞ is the initial shear module, η_0 is the viscoelastic constant, and β is the decay constant (Table 1).

Given the inconsistency of reported bulk moduli, varying over a 10^3 factor (Table 2), an inverse-engineering approach was adopted to overcome the uncertainty pertinent to the equation of state, the dynamic constitutive response, and the triaxial response to the stress of biological tissues.

Computational model parameters were tuned to reproduce the experimental data of Delori et al.,[9] by running multiple simulations and varying one modulus value at a time. Parametric analyses of bulk moduli were conducted by cross-matching simulation curves with Delori's results of corneal indentation (Fig. 3) and BB pellet rebound speed (Figs. 4, 5).

Once the computational model was finalized, the mechanical response to a standardized impact was simulated in both vitreous and aqueous-filled eyes (Fig. 5). Main outcome measures included pressure, strain, and strain rates.

Positive (compression) and negative (traction) pressures as a function of time from impact (t_0) were calculated, with special regard to the areas where damage is clinically more evident: the macula and

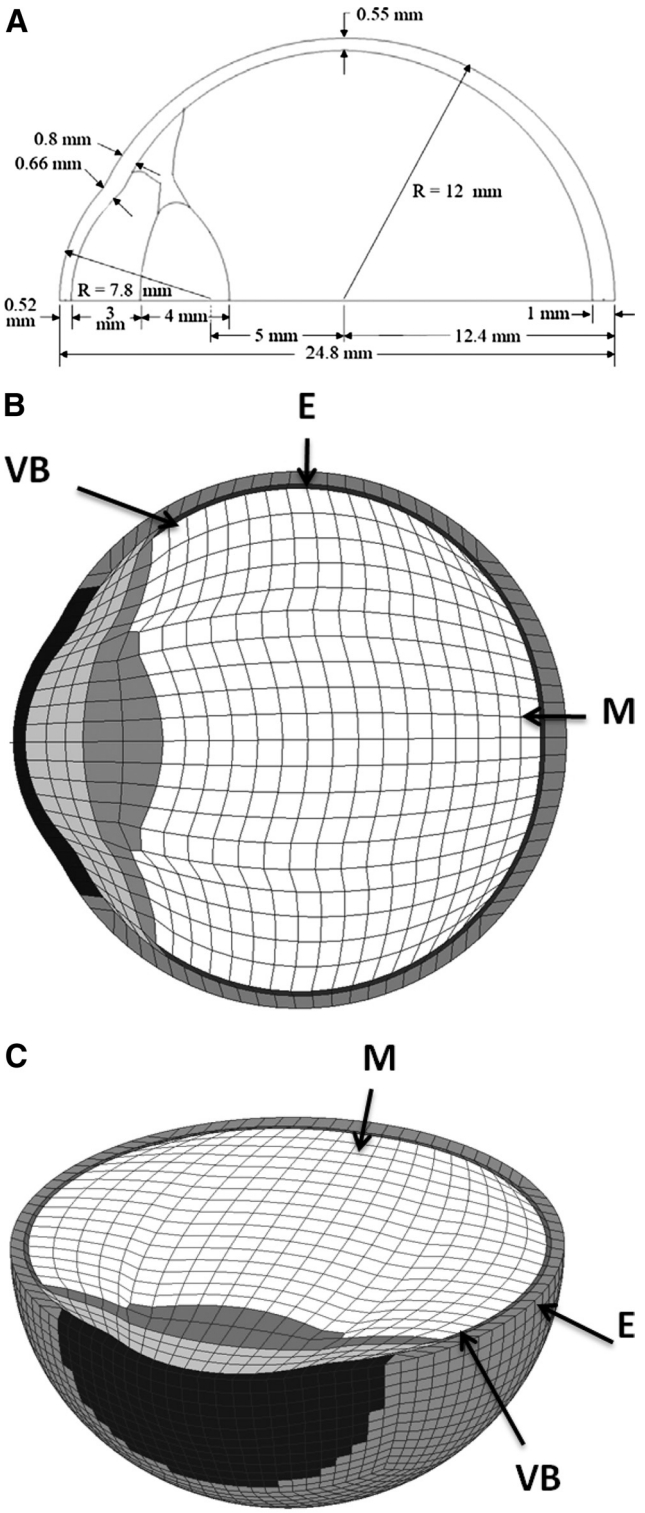

FIGURE 2. Eye model and FEM mesh. (**A**) Ideal eye model. Dimensions, thickness, and radius of curvature are reported. An FEM mesh of the generic eye shown in anteroposterior (**B**) and 3D (**C**) sections. The mesh consisted of 6912 nodes and hexahedral elements. Anatomic landmarks used for retinal strain and pressure measurement: VB, vitreous base; M, macula; E, equator. See Table 1 for the constitutive models and mechanical properties used by the numerical simulation.

TABLE 1. Constitutive Models and Mechanical Properties of FEM

Material	Constitutive Model	Young Modulus (MPa)	Shear Modulus (MPa)	Poisson Modulus	Bulk Modulus (MPa)	Density (kg/m^3)
Sclera	Linear elastic	28.0	—	0.49	—	1200
Cornea	Linear EOS + shear modulus	1.5	0.5	—	300	1143
Lens	Linear EOS	—	—	—	1000	1100
Retina	Linear EOS + shear modulus	—	0.035	—	1000	1100
Aqueous	Linear EOS	—	—	—	2200	1000

Material	Constitutive Model	G_0 (MPa)	G_∞ (MPa)	Viscosity η_0 (MPa)	Decay Constant	Bulk Modulus (MPa)	Density (kg/m$_3$)
Vitreous	Linear EOS + linear shear viscoelastic	$10e^{-6}$	$2e^{-6}$	$5e^{-6}$	0.01	2000	950

EOS, equation of state.

vitreous base. The retinal equator location was also calculated as a reference.

Strain was calculated on the retinal surface by means of an algorithm provided in the software (PATRAN; MSC Software). Logarithmic or true strain (ε) is commonly defined as

$$\varepsilon = \ln\left(1 + \frac{\Delta l}{l_0}\right)$$

where Δl is the incremental elongation and l_0 is the initial reference length. True strain of solid elements is commonly reported as principal strain along three orthogonal axes (max, mid, and min), whereas the net result of the three vectors composition at each given time point is reported as the algebraic sum and referred to as the "trace of the elastic strain tensor," which can also be regarded as the percentage of volume variation for each tridimensional tissue element.

Strain rate is defined as its derivative with respect to time

$$\frac{d\varepsilon}{dt}$$

Displacement velocity, defined as deformation over time (expressed in millimeters per second) was also calculated.

A reduced integration scheme (i.e., one Gauss point per element) has been used to prevent locking phenomena (as for the sclera, where the Poisson ratio approaches 0.5), and to achieve low-cost formulation. Consequently, we used a viscous form of hourglass control, available in the software (DYTRAN; MSC Software),[27] to control 0 energy deformation modes and to avoid overstiffening of the element.

The timeframe covered during the simulation spans 1 ms after the BB pellet contacts the corneal apex (Fig. 6; Supplementary Movie S1, http://www.iovs.org/lookup/suppl/doi:10.1167/iovs.10-6477/-/DCSupplmental), because most of the phenomenon is over at this time point, and only minor oscillations were described by Delori et al.[9] thereafter.

TABLE 2. Elastic Moduli Reported in the Literature

Cornea	Sclera	Retina	Vitreous
0.05–0.4[16]	0.15–0.83[16]	0.02[17]	2.8[18]
0.07–0.29[19]	0.2–0.5[20]		7.0[18]
0.2–2[21]	2.6[22]		
0.3–50[22]	2.9[23]		
2.87–19[24]	358[19]		
124[25]			
1300[26]			

Data are reported in megapascals.

For purposes of clarity, the phenomenon was arbitrarily divided into two phases: a compression phase, from the initial contact ($t = 0$) up to the time at which the BB pellet is arrested ($V = 0$; which occurs at 0.28 ms after t_0), and a rebound phase (from 0.28 to 1 ms). Beyond this time point, the analysis was interrupted due to subsequent interaction and reverberation of reflected stress waves.

Statistical Analysis

Statistical analysis used paired-samples *t*-tests to compare pressure and strain values in vitreous- and aqueous-filled eyes. Significance was set at 0.05.

RESULTS

The BB produced a maximum corneal indentation of 8.5 mm, 0.28 ms after contact (t_0; Fig. 3A). Force at impact was 217 N and energy delivered was 0.68 J. BB pellet speed reached 0 at 0.28 ms after t_0. Rebound maximum speed was −11.4 m/s, and the amount of energy dissipated by the impact was 94.6%.[9] Snapshots of FEM simulations taken every 0.1 ms from corneal contact (t_0) are reported in Figure 6. Pressure variations at the macula, vitreous base, and retinal equator in vitreous- and aqueous-filled eyes are reported in Figure 7. Paired *t*-test analysis showed a significant pressure difference between the vitreous- and aqueous-filled eyes at the macula during the compression phase only ($P < 0.0001$), whereas no significant differences were found at any examined location during the entire rebound phase. It should be noted, however, that peak negative pressure at the vitreous base was reached at 0.35 ms (Table 3), thus the "rebound" phase at the vitreous base seems to lag behind the corneal rebound and starts at this very moment. Of note, when the paired *t*-test was run for the time-frame between 0.36 and 1 ms, the difference between vitreous- and aqueous-filled eyes pressures at the vitreous base yield statistically significant results ($P = 0.04$).

Compression and traction peak pressures at the vitreous base, equator, and macula are reported in Table 3 for both vitreous and aqueous-filled eyes and ranged between −1 and +2 MPa (i.e., −7,600 and +14,440 mm Hg).

Strain is reported in Figure 8 for both vitreous and aqueous-filled eyes. Peak strain along multiple axes reached 20% at the macula and 25% at the vitreous base in aqueous-filled eyes and slightly less in vitreous-filled eyes. Paired *t*-tests returned significantly higher strain values for aqueous-filled eyes at the macula, equator, and vitreous base for each calculated axis (in all cases $P < 0.001$). The trace of the elastic strain tensor is shown in Figure 9. The difference between vitreous- and aqueous-filled eyes was not significant at the macula, equator, or vitreous base ($P = 0.23$, $P = 0.11$, and $P = 0.18$, respectively).

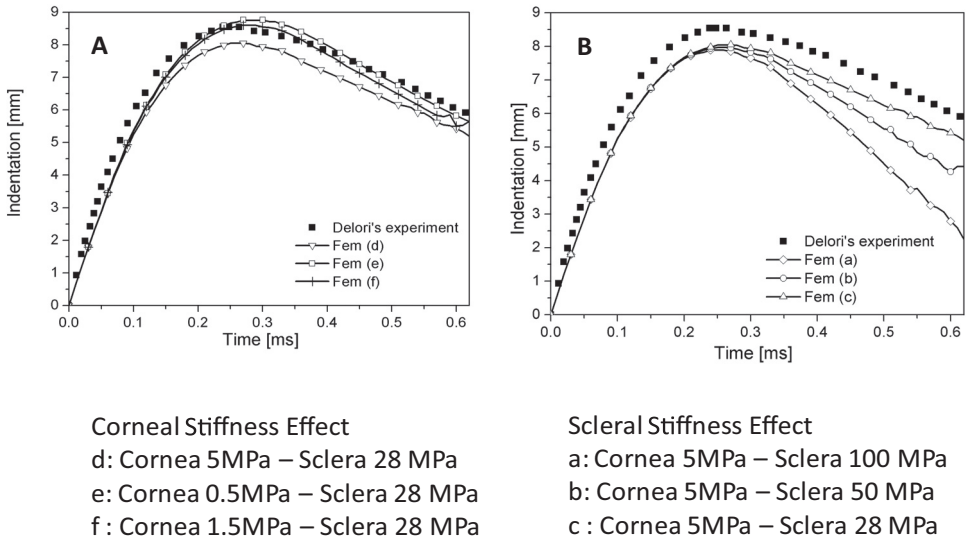

FIGURE 3. Plot of corneal apex indentation as a function of time. Corneal (**A**) and scleral (**B**) stiffness variation effects are reported independently parametrically, by modifying one modulus at a time until Delori's experimental data are matched. Different curves represent the referral Delori data and FEM simulation according to different hypothesis. Curves (a), (b), and (c) retain the same corneal shear modulus of 5 MPa, whereas scleral Young's modulus varies from 100 to 50 to 28 MPa, respectively (**B**), and curves (d), (e), and (f) maintain a fixed scleral Young's modulus of 28 MPa while varying the corneal shear modulus from 5 to 0.5 to 1.5 MPa (**A**).

Strain rate (Fig. 10) peaked at 50,000 seconds^{-1} at the vitreous base, 57,000 seconds^{-1} at the equator, and 40,000 seconds^{-1} at the macula, with significantly higher values for aqueous-filled eyes at each investigated location ($P < 0.0001$ in all cases). Calculated displacement velocity varied between 5,000 and 10,000 mm/s.

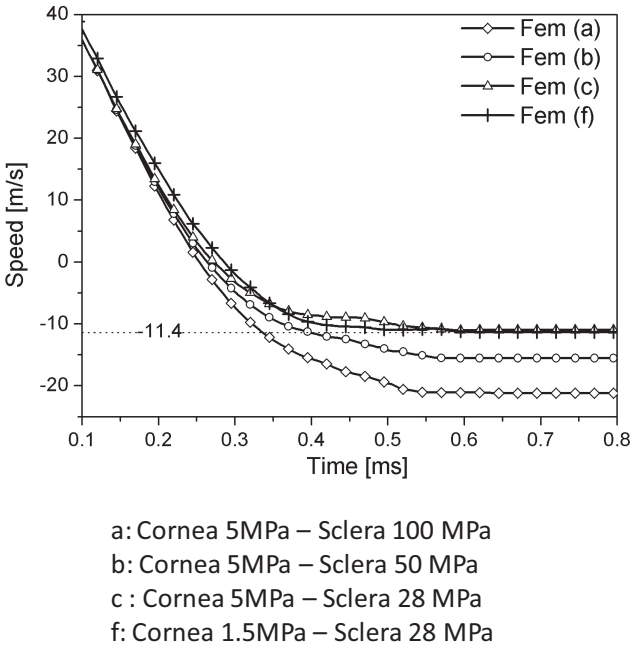

FIGURE 4. BB speed plot as a function of time. The four curves report FEM simulation data according to different hypothesis: (a) corneal shear modulus of 5 MPa, scleral Young's modulus of 100 MPa; (b) cornea percentage of MPa, sclera 50 MPa; (c) cornea 5 MPa, sclera 28 MPa; (f) cornea 1.5 MPa, sclera 28 MPa. The *dotted horizontal line* at −11.4 m/s velocity indicates the rebound speed according to Delori et al.[9]. Only curves (c) and (f) replicate the rebound speed of −11.4 m/s of Delori's experiment, although the (c) scleral and corneal moduli values did not fit Delori's corneal indentation curve (see Fig. 3A) and were therefore discarded.

DISCUSSION

The study was prompted by the anecdotal observation of MH and peripheral retinal edema after a BB injury in a previously vitrectomized eye. Although most accredited theories infer that vitreous strands pull on the vitreous base and the macula when the eye is deformed, our patient represents the proof of principle that retinal lesions may also develop in the absence of vitreous, suggesting that alternative pathogenic pathways should be sought. To study whether shockwave propagation, per se, can induce retinal damage, regardless of the presence of vitreous, we simulated a blunt trauma, focusing on pressure, strain, and strain rate.

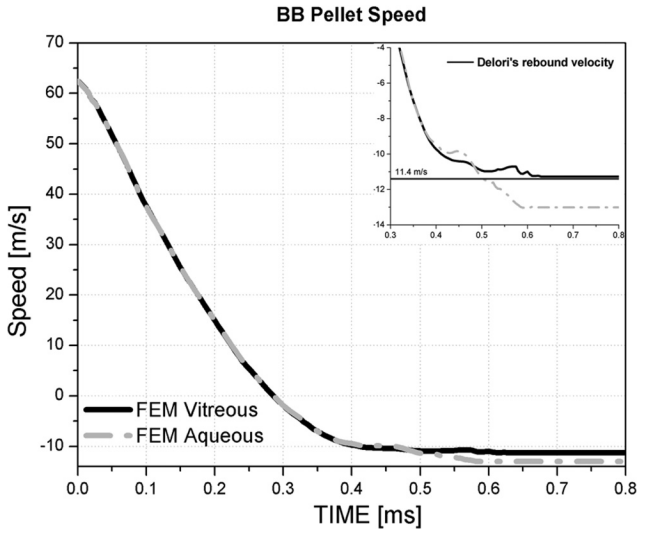

FIGURE 5. The BB's speed plotted as a function of time from corneal contact (t_0) assuming a corneal Young's modulus of 1.5 MPa and scleral Young's modulus of 28 MPa, simulated in vitreous (*solid black curve*) and aqueous-filled eyes (*dashed gray curve*). The upper right quadrant shows at a different scale the rebound speed difference, indicating a significantly higher negative speed in aqueous-filled eyes.

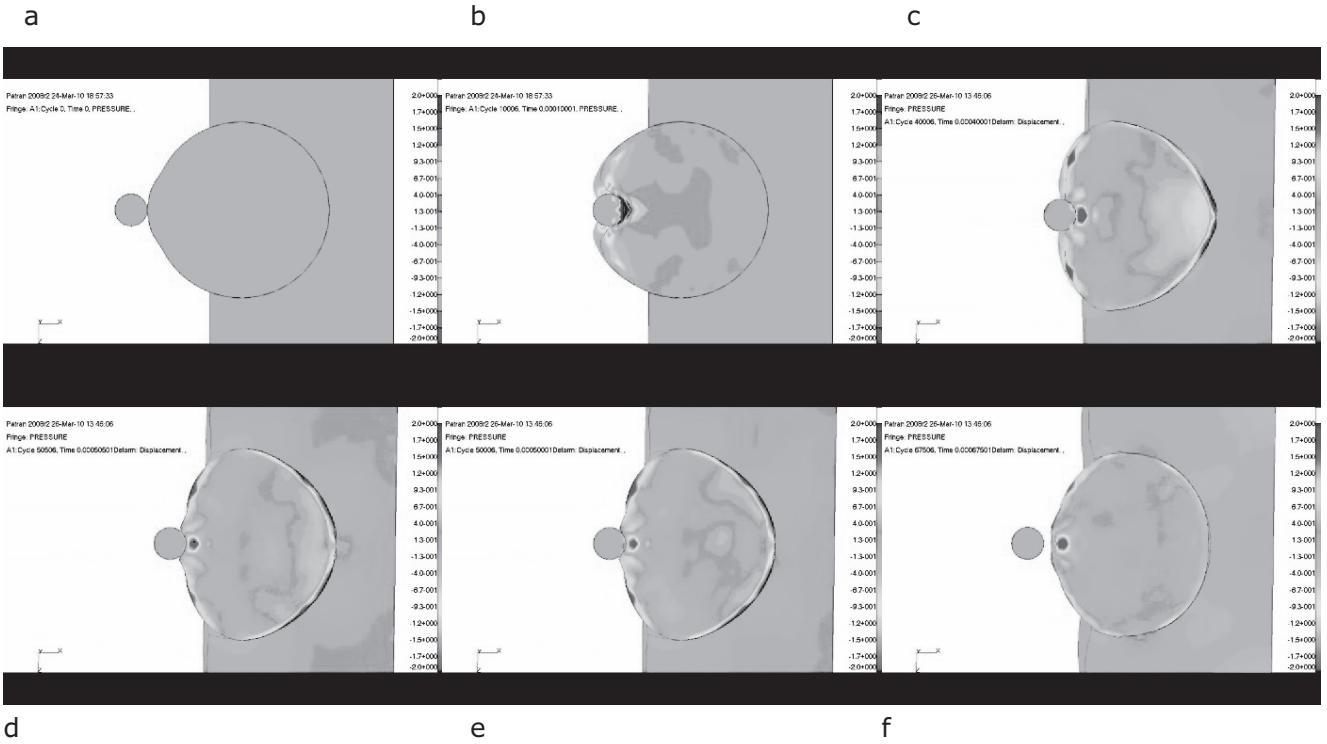

FIGURE 6. FEM analysis snapshots from corneal contact to rebound phase, taken at 0.1-ms intervals: (**a**) t_0 (the BB pellet contacts the corneal apex); (**b**) 0.1 ms after t_0, (**c**) 0.28 ms (at this time point, the BB pellet speed is 0 and the rebound phase starts), (**d**) 0.4 ms, (**e**) 0.5 ms, and (**f**) 0.6 ms from impact (t_0).

Constructing a mathematical model of the eye proved extremely difficult, due to the lack or inconsistency of eye mechanical properties data (see Table 2).[28,29] and intrinsic complexity. While mesh geometry of an ideal eye can be drawn with relative ease, in fact, constitutive response data often derive from in vitro experiments of isolated tissues, and some are simply missing.[16,23,30]

Probably the major difficulty in constitutive modeling of soft tissues is that it is impossible to rely on published data of the effective material stress–strain response obtained under controlled sample geometry and loading conditions. The thinness of the tissue layers and the lack of homogeneity and isotropy in their structures make characterization testing very challenging and may explain the large disparity in the values and moduli reported in the literature (Table 2). Although several sophisticated constitutive model formulations for hyperelastic-visco-plastic materials are available in the literature, the use of the models is made difficult by the large number of parameters that have to be identified.[31–33]

In this study, due to the complexity of the problem (e.g., different tissue types, multiaxial state of stress conditions, and high strain rate deformation process), as far as constitutive modeling is concerned, Occam's Razor law was applied: "entia non sunt multiplicanda praeter necessitatem"—that is, to use the simplest reasonable assumptions to explain (or in our case to reproduce) a given phenomenon.

Therefore, we decided to use simple constitutive models (such as linear-elastic laws and linear equation of states) and to tune the model parameters on the milestone experiment of Delori et al.,[9] by using a reverse-engineering approach, to reproduce their results. Once properly calibrated, the constitutive model was used to investigate the response in both vitreous- and aqueous-filled eyes, to calculate pressure and strain variations.

One could argue that simplifying the constitutive model may affect the accuracy of calculated pressure and strain values. However, it should be considered that if the proposed constitutive and computation model can reproduce accurately amplitude and time response measured under controlled impact conditions,[9] there is no reason to believe that the calculated values should differ from those obtained in the experimental setting.

Pressure at the retinal surface ranged between +1.9 and −1.0 MPa (Fig. 6, Table 3)—values that look exceedingly high when compared to eye pressure at rest (close to 0.02 MPa), but appear realistic when considering that experiments on scleral rupture pressures report values between 1 and 13 MPa.[17,19,34] The clinical relevance of high positive pressure for less than 1 ms remains a matter of speculation, although it seems reasonable to assume that mechanical deformation, ischemia, and axon flux interference can all contribute to retinal and choroidal damage. Such damage, being mediated by physiologic factors (i.e., ischemia, axonal transport, and perfusion) would most likely take time to become patent and is probably responsible for the subacute and chronic manifestation of blunt trauma: retinal ischemia and RPE mottling.

Negative pressures play, in our opinion, an even more critical role in retinal adherence and integrity. Compression (i.e., positive pressure), in fact, pushes the retina and choroid against the much stiffer sclera, which limits deformation (and possibly damage), whereas traction (i.e., negative pressure) pulls the retina toward the center of the vitreous chamber with the sole adhesive force of the retinal pigment epithelium and the retina's tensile strength counteracting its tendency to detach and tear.

The key question therefore is: Can this "traction" pressure, in combination with strain, detach and/or tear the retina? Wollensak et al.[35,36] measured retinal stress at a failure of 9 kPa

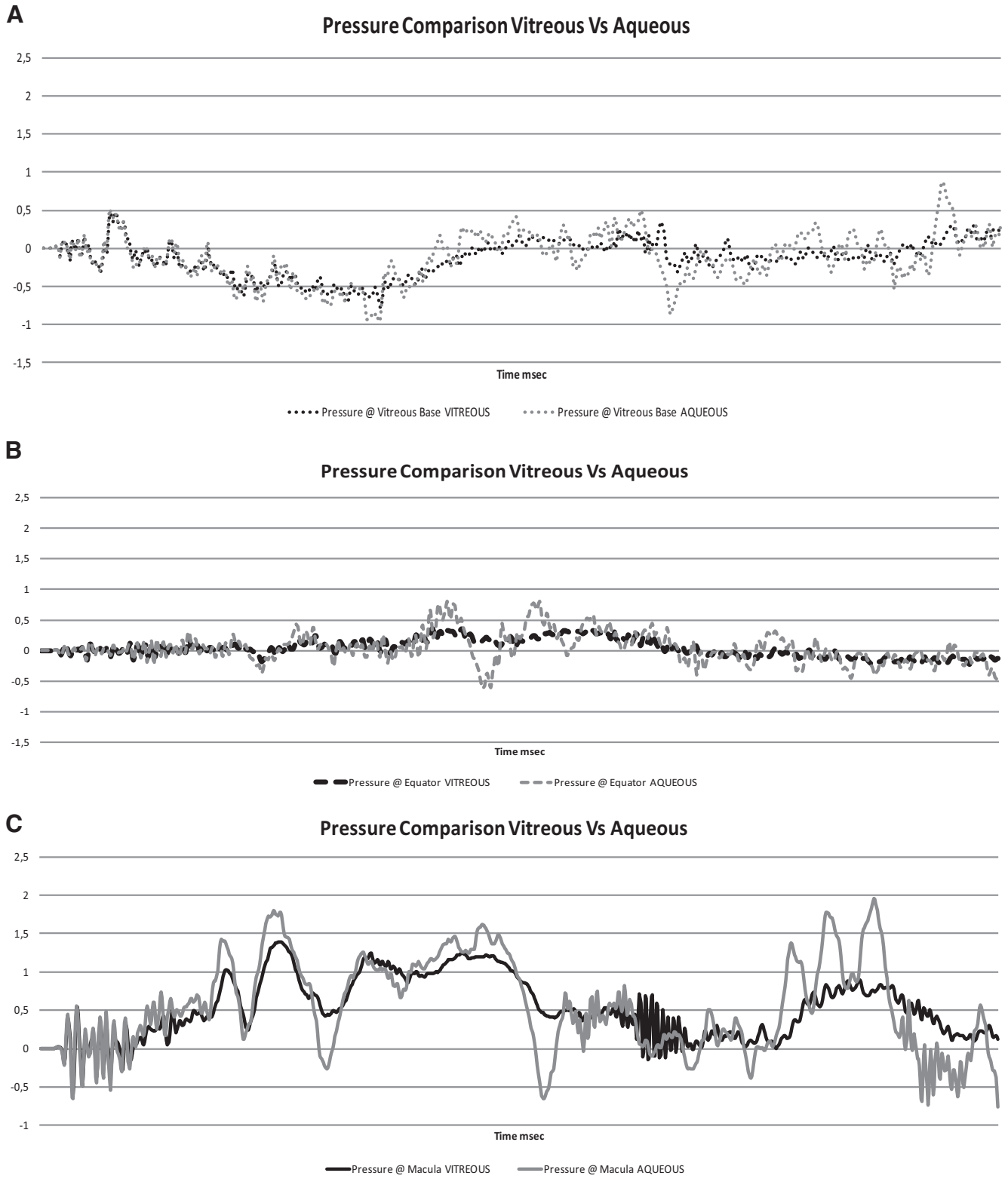

FIGURE 7. Pressures as a function of time at the vitreous base (**A**), equator (**B**), and macula (**C**). Pressures in the aqueous-filled eyes tended to reach higher values, both positive and negative (paired *t*-test: $P < 0.0001$ in all three pairs), at all locations. The macula was exposed to the highest positive (compression) peaks, whereas the vitreous base mainly had negative pressure (traction). The equator is exposed to lower pressure, both positive and negative, especially with vitreous in the vitreous chamber.

at 0.03 mm/s, which rose to 11 kPa when load rate increased to 1.65 mm/s, whereas the strain of isolated retinal strips reduced from 80% to 50%. Wu et al.[37] calculated a reference Young's modulus in simple uniaxial elongation of 5 kPa, whereas Friberg[16] determined values of stress at failure for isolated choroid strips of 300 kPa. Similar results, although difficult to compare due to significant mismatch of the respective experimental settings, are several orders of magnitude

TABLE 3. Peak Pressure Values at the Macula, Equator, and Vitreous Base and Relative Time after Impact

	Macula				Equator				Vitreous Base			
	Vitreous		Aqueous		Vitreous		Aqueous		Vitreous		Aqueous	
	MPa	$t - t_0$	Mpa	$t - t_0$	Mpa	$t - t_0$	Mpa	$t - t_0$	Mpa	$t - t_0$	Mpa	$t - t_0$
Peak negative pressure	−0.6	0.03	−0.6	0.53	−0.2	0.97	−0.6	0.46	−0.8	0.35	−1	0.35
Peak positive pressure	1.3	0.25	1.8	0.86	0.4	0.44	0.8	0.52	0.5	0.08	0.5	0.07

$t - t_0$ data are expressed in milliseconds.

lower than the pressures we calculated. We therefore propose that negative pressure can conceivably both tear and detach the retina.

Retinal strain values peaked at 20% to 25% along different axes (Fig. 7), for both the macula and vitreous base, with strain rates up to 30,000 seconds^{-1} for the macula and over 50,000 seconds^{-1} for the vitreous base (Fig. 9) and a displacement velocity between 5,000 and 10,000 mm/s. The question of whether those values are capable of ripping the retina is a difficult one. Wollensak et al.[35,36] reported a much higher strain at failure of 51% at 1.6 mm/s, whereas Wu et al.[37] measured extension ratios of isolated animal retina strips between 1.7 and 1.9, calculated at extremely low displacement velocity varying between 0.36 and 3.60 mm/sec. Jones et al.[23] calculated a Young's modulus of 20 kPa for the isolated retina. Because of inconsistency in the methods, these data also are hardly comparable and may be not be representative of the eye response. Extrapolating data from isolated tissues, in fact, warrants extreme caution, especially because the retina, choroid and sclera all show nonlinear, anisotropic, and inhomogeneous mechanical characteristics[25,29] and living, perfused organs can behave in a significantly different way. It must be noted, however, that the strain rates and displacement velocity that we measured along multiple axes (Figs. 9, 10) are more than 10^3 times higher than most reported experimental data. Several classes of materials show a strain rate effect on the constitutive response (i.e., an increased stress value at the same strain level for higher strain rates), but the same cannot be inferred for strain-to-failure values that may either increase or decrease as a function of the strain rate. In any case, we were able to measure a high level of stress multiaxiality (measured by the ratio of the hydrostatic and the deviatoric part of the stress tensor), which is known to reduce drastically the material strain to failure.[38] We therefore propose that multiaxial strain also participates in the pathogenesis of anterior and posterior retinal lesions.

A further question is: Why does blunt trauma damage localize at the macula and vitreous base? In the presence of vitreous, this phenomenon is generally explained as the consequence of constraints due to preferential vitreous-retinal adhesion sites. Wu et al.[37] and Chen et al.[25] found that isolated retinal strips containing retinal vessels are significantly stiffer than strips with no visible vessels, possibly due to the presence of the elastic tunica. The fovea is avascular, and the vitreous base contains very few vessels; the retina can therefore be regarded as a series of elements whose differential stiffness may force the most elastic ones (vitreous base and macula) to deform more and possibly reach the breaking point earlier when stress is applied. We also showed that both positive and negative pressures were higher at the macula and vitreous base than at the equator (Fig. 6, Table 3), and this could add a further reason for localizing damage in such areas. Based on this assumption, strain does not seem to explain the preferential location of retinal damage at the vitreous base and macula, since peak values did not differ significantly. Multiaxial strain

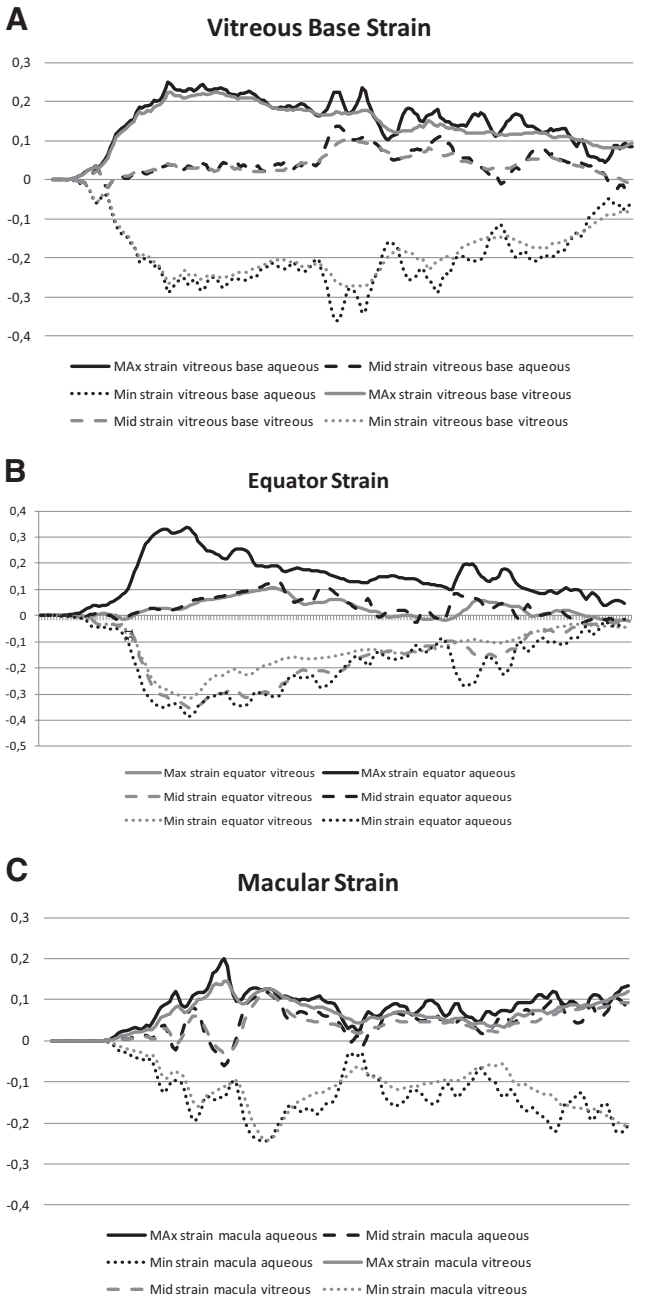

FIGURE 8. Principal strain values along three principal orthogonal axes (max, mid, and min) calculated in vitreous- and aqueous-filled eyes at the vitreous base (**A**), equator (**B**) ,and macula (**C**). At all locations that showed strain multiaxiality, there was simultaneous positivity of strain values along two axes (max and mid).

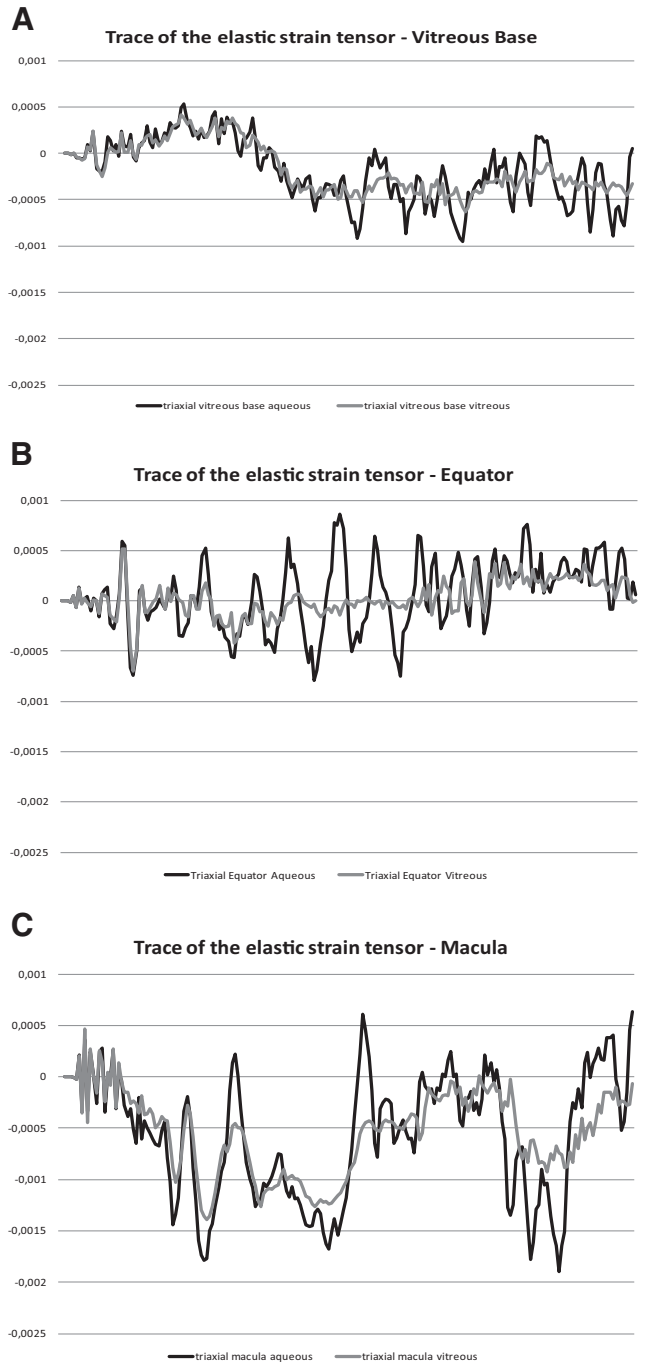

FIGURE 9. Trace of the elastic strain tensor graph (i.e., percentage of volume change as a function of time) at the vitreous base (**A**), equator (**B**), and macula (**C**). Each point is calculated as the algebraic sum of max, mid, and min principal strain (see Fig. 8) at each time point and represents the net effect of strain on each solid element. Positive values indicate a volume increase whereas negative values are a contraction. The graphs show marked deformation, both positive and negative, for the first 0.1 ms, after which the vitreous bases and macula behave in opposite ways, up to 0.5 ms.

patterns over the time and the trace of the elastic tensor (Figs. 8, 9), instead, differed overtly, although we are unable to assign a clinical significance to such behavior.

In summary, on the basis of our patient's experience and the FEM results, we believe that we should reconsider the role of vitreous in high-speed blunt trauma. Although it is apparent that it may not play a key pathogenic role in the development of both macular and peripheral lesions, for the simple reason that our vitrectomized patient experienced both, the question of whether it plays any protective role is an intriguing one and needs to be resolved. We indeed measured significantly lower values of pressure, strain, and strain rate in vitreous-filled eyes (Figs. 7, 8), presumably due to the lower bulk modulus. The

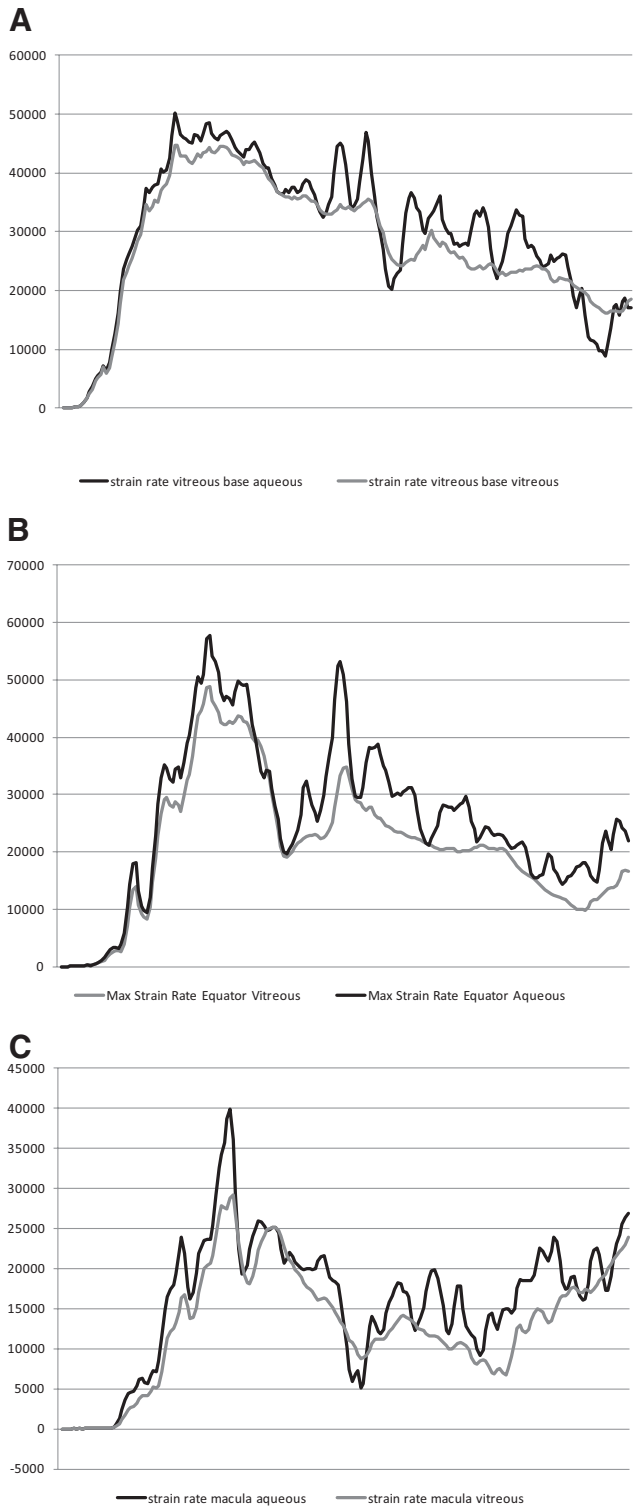

FIGURE 10. Strain rate at the vitreous base (**A**), equator (**B**), and macula (**C**) in aqueous- and vitreous-filled eyes. Values for aqueous-filled eyes were significantly higher at all locations (paired *t*-test $P < 0.001$).

presence of aqueous in the vitreous chamber also yielded a significantly higher BB pellet rebound speed (Fig. 5), as expected.

From a merely structural point of view, it can be assumed that viscoelastic damping capability[18,20,31] reduces pressures and therefore strain and perhaps, damage. Whether this statistically significant difference translates into a real-life clinical protective effect, especially when impacts generating such high pressures are considered, remains unclear and is probably true only for much lower pressures at which the vitreous damping role is intended to function.

As a conclusion, while we acknowledge the many pitfalls of the present study related to the lack of experimental data on tissue mechanical response and equations of state of the eye as a whole, we propose that the eye's constitutive response to shockwave propagation is the main pathogenic mechanism of both the anterior and posterior retinal lesions associated with high-speed blunt traumas. The limitations related to the simplification of our constitutive model included the attribution of linear elastic properties to tissues such as the sclera and retina that are known to be anisotropic and inhomogeneous,[27] at least to some extent. However, as discussed in the paper, due to the lack of information about the effective response of these materials under complex stress states, dynamic pressure, and deformation (strain rate sensitivity), it seemed reasonable to approach the problem by limiting the number of unknown constitutive parameters, to ensure that the optimized set found by reverse engineering of the Delori experiment was unique and the best suited. Further research is warranted in the field of applying FEM to biological systems. We believe the refinement of mathematical models will undoubtedly participate in a substantial improvement of our knowledge of eye trauma.

References

1. Kuhn F, Morris R, Whiterspoon CD, Heimann K, Jeffers J, Treister G. A standardized classification of ocular trauma terminology. *Ophthalmology.* 1996;103:240–243.
2. Ligget Pe, Pince KJ, Barlow W, et al. Ocular trauma in an urban population: review of 1132 cases. *Ophthalmology.* 1990;97:581–584.
3. Sternberg P Jr. Trauma: principles and techniques of treatment. In: Ryan SJ, ed. *Retina*. 2nd ed, vol 3. St Louis: Mosby; 1994:2351–2378.
4. Berlin R. Zur sogenaunten commmotio retinae. *Klin Monatsbl Augenheilkd***.** 1873;1:42–78.
5. Von Graefe A. Zwei falle von rupture der choroidea. *Graefes Arch Ophthalmol***.** 1854;1:402–403.
6. Dumas JJ. Retinal detachment following contusion of the eye. *Int Ophthalmol Clin.* 1967;7:19–38.
7. Margherio RR, Schepens CL. Macular breaks: diagnosis, etiology and observations. *Am J Ophthalmol.* 1972;74:219–222.
8. Cooling RJ. Traumatic retinal detachment mechanisms and management. *Trans Ophthalmol Soc UK.* 1986;105:575–579.
9. Delori F, Pomerantzeff O, Cox Ms. Deformation of the globe under high speed impact: its relation to contusion injuries. *Invest Ophthalmol*. 1969;8:290–301.
10. Kuhn F, Morris R, Mester V, Witherspoon C. Internal limiting membrane removal for traumatic macular holes. *Ophthalmol Surg Lasers.* 2001;32:308–315.
11. Roberts MD, Liang Y, Sigal IA, et al. Correlation between local stress and strain and lamina cribrosa connective tissue volume fraction in normal monkey eyes. *Invest Ophthalmol Vis Sci.* 2010; 51(1):295–307.
12. Gefen A, Shalom R, Elad D, Mandel Y. Biomechanical analysis of the keratoconic cornea. *J Mech Behav Biomed Mater.* 2009;2(3): 224–236.
13. Amini R, Barocas VH. Anterior chamber angle opening during corneoscleral indentation: the mechanism of whole eye globe deformation and the importance of the limbus. *Invest Ophthalmol Vis Sci.* 2009;50(11):5288–5294.
14. Capstick PH. *Death in a Lonely Land: More Hunting, Fishing, and Shooting on Five Continents*. New York: Macmillan; 1990.
15. Snell RS, Lemp MA. *Clinical Anatomy of the Eye*. 2nd ed. New York: Blackwell Science, Inc.; 1998:214–231.
16. Friberg T. A comparison of the elastic properties of the human choroid and retina. *Exp Eye Res.* 1988;47:420–436.
17. Stitzel JD, Duma SM, Cormier JM, et al. A nonlinear finite element model of the eye with experimental validation for the prediction of globe rupture. *Stapp Car Crash J.* 2002;46:81–102.
18. Lee B, Litt M, Buchsbaum G. Rheology of the vitreous body. Part I: viscoelasticity of human vitreous. *Biorheology.* 1992;29:521–533.
19. Bullock JD, Warwar JE, Green RW. Ocular explosions from periocular anesthetic injections: a clinical, histopathologic, experimental, and biophysical study. *Ophthalmology.* 1999;106:2341–2353.
20. Nickerson CS, Park C, Kornfield JA, Karageozian H. Rheological properties of the vitreous/ and the role of hyaluronic acid. *J Biomech.* 2008;41:1840–1846.
21. Elsheikh A, Geraghty B, Alhasso D, Knappett J, Campanelli M, Rama P. Regional variation in the biomechanical properties of the human sclera. *Exp Eye Res.* 2010;90:624–633.
22. Schultz DS, Lotz JC, Lee SM, Trinidad ML, Stewart JM. Structural factors that mediate scleral stiffness. *Invest Ophthalmol Vis Sci.* 2008;49:4232–4236.
23. Jones IL, Warner M, Stevens JD. Mathematical modeling of the elastic properties of retina: a determination of Young's modulus. *Eye.* 1992;6:556–559.
24. Hjortdal JO. Regional elastic performance of the human cornea. *J Biomech*. 1996;29:931–942.
25. Chen K, Weiland JD. Anisotropic and inhomogeneous mechanical characteristics of the retina. *J Biomech.* 2010;43(7):1417–1421.
26. Smolek MK. Holographic interferometry of intact and radially incised human eye-bank corneas. *J Cataract Refract Surg.* 1994;20: 277–286.
27. *MSC/Dytran LS-Dyna User's Manual*. Santa Ana, CA: MCS Software; 2009.
28. Girard MJ, Downs JC, Burgoyne CF, Suh JK. Peripapillary and posterior scleral mechanics, Part I: development of an anisotropic hyperelastic constitutive model. *Biomech Eng.* 2009;131(5): 051011.
29. Uchio E, Ohno S, Kudoh J, et al. Simulation model of an eyeball based on finite element analysis on a supercomputer. *Br J Ophthalmol.* 1999;83:1106–1111.
30. Asejczyk-Widlicka M, Pierscionek BK. The elasticity and rigidity of the outer coats of the eye. *Br J Ophthalmol*. 2008;92:1415–1418.
31. Zimmerman RL. In vivo measurements of the viscoelasticity of the human vitreous humor. *J Biophisics.* 1980;29:539–544.
32. Pierscionek BK, Asejczyk-Widlicka M, Schachar RA. The effect of changing intraocular pressure on the corneal and scleral curvatures in the fresh porcine eye. *Br J Ophthalmol.* 2007;91:801–803.
33. Wang H, Prendiville PL, McDonnell PJ, Chang WV. An ultrasonic technique for the measurement of the elastic moduli of human cornea. *J Biomech.* 1996;29(12):1633–1636.
34. Bisplinghoff JA, McNally C, Duma SM. High-rate internal pressurization of human eyes to predict globe rupture. *Arch Ophthalmol.* 2009;127(4):520–523.
35. Wollensak G, Spoerl E, Grosse G, Wirbelauer C, Biomechanical significance of the human internal limiting lamina. *Retina.* 2006; 26:965–968.
36. Wollensak G, Spoerl, E. Biomechanical characteristics of retina. *Retina.* 2004;24:967–970.
37. Wu W, Peters WH, Hammer ME. Basic mechanical properties of the retina in simple elongation. *J Biomech Eng.* 1987;109:65–67.
38. Bonora N. On the effect of triaxial state of stress on ductility using nonlinear CDM model. *Int J Fracture.* 1997;88:359–371.